

MULTILEVEL DETECTION OF DAMAGE AND REPAIR IN HEALABLE POLYMER-MATRIX COMPOSITES

G. LACIDOGNA ^{*†}, B. CHIAIA ^{*†}, G. PIANA ^{*†}, E. SILVA CEZAR ^{*} AND F. VECCHIO ^{*}

^{*} Politecnico di Torino, Department of Structural, Geotechnical and Building Engineering,
Corso Duca degli Abruzzi 24, 10129 Torino, Italy
e-mail: giuseppe.lacidogna@polito.it; bernardino.chiaia@polito.it; gianfranco.piana@polito.it;
ediblu.silvacezar@polito.it; federico.vecchio@polito.it, www.polito.it

[†] Politecnico di Torino, Interdepartmental Center SISCON - Safety of Infrastructures and Constructions,
Corso Duca degli Abruzzi 24, 10129 Torino, Italy
e-mail: giuseppe.lacidogna@polito.it; bernardino.chiaia@polito.it; gianfranco.piana@polito.it,
www.siscon.polito.it

Key words: Composites, Damage, Self-healing, Acoustic Emission Technique, Digital Image Correlation, Tensile Test

Abstract: We present some results obtained in the ongoing research project entitled “*IN MOOSHEAC - INnovative damage MONitoring Of Self-HEaling Composites by acoustic emission in civil and aerospace applications*”. The research program aims at utilizing Nondestructive Evaluation (NDE) techniques for monitoring the healing process of healable composites and to investigate their structural properties post healing. In this campaign, samples of composite thin rectangular strips were designed and manufactured on purpose, and then tested in the lab under tension. The samples were supplied by a company that has developed a new type of resin - HealTech™ - giving composite materials the ability to heal micro cracks and delamination in about one minute after a localized heat supply. Acoustic Emission (AE) technique was used to detect damage, while Digital Image Correlation (DIC) was adopted to measure surface deformation. Data from both techniques were employed to assess material repair.

1 INTRODUCTION

In this work, a type of self-healing material is under study. This type of smart material presents the ability to partially or fully restore its original properties after suffering mechanical damage, such as micro cracks, delamination etc., which can lead to component failure [1,2].

In this specific case, a carbon fiber (CF) polymeric composite that has the repair mechanism activated by locally heating the damaged region in a range of 100°C–150°C, is analyzed by destructive and non-destructive techniques.

It is worth pointing out that the main objective of this work is to evaluate the mechanical behavior of the composite under investigation, both before and after the repair process, but not to evaluate whether the repair process is effective or not.

For the analyses, non-destructive techniques such as DIC (Digital Image Correlation) and AE (Acoustic Emission) were employed in addition to tensile testing [3]. The above-mentioned techniques have already been applied to evaluate composite materials, specifically with repair characteristics, with very good results. Regarding to mechanical tests, tapered double-cantilever beams were

tested under controlled displacement, up to failure, measuring compliance and peak load in [4]. In [5] AE was applied for the monitoring *in situ* of two repaired composite panels. The AE technique was effective in detecting the damage type by similar frequencies. In the work [6], the AE technique was also employed, along with tensile test, to linear localization of crack tip in pre-delamination of laminated composites. According to the authors, the AE was able to predict delamination growth in laminated composite. It is known that the DIC technique works well alongside with tensile tests. In this way, the DIC technique was employed in [7] to evaluate the mechanical tensile response of bio-mimicking (3D)-printed polymers.

2 MATERIALS AND METHODS

The study utilizes a multilayer composite made from carbon fibers (T700 UD), which includes an interleaved film aimed at restoring or improving adhesion between layers via a heating process at temperatures between 100 and 150°C for several minutes. This film is composed of particles from thermosetting components that are distributed within a thermoplastic matrix. The thermosetting particles, sized between 0.1 and 15 micrometers, should preserve their structural integrity when subjected to heat, whereas the thermoplastic component begins to soften at a temperature that is lower than the decomposition temperature of both the particles and the other layers of the material. The material, which is referred to in commercial terms as HealTech™, was acquired from CompPair (Switzerland).

2.1 Samples

The samples analyzed (Figure 1) consisted of strips with the following average dimensions: 25 mm on the short side, 250 mm on the long side, and a thickness of 3.5 mm. The sample comprised a double layer of carbon fibers arranged in the orientations of 45°/0°/-45°/90°.

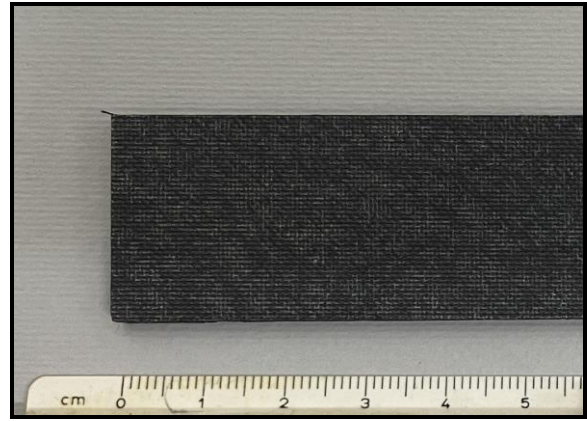


Figure 1: Detail of one of the specimens utilized.



Figure 2: Detail of test setup and apparatus.

2.2 Setup and techniques

The samples underwent three distinct tests concurrently (Figure 2): tensile tests in displacement control utilizing a servo-hydraulic universal machine by MTS equipped with a 100 kN load cell; acoustic emission (AE) technique employing a single sensor (model LT18-003-PRD00-R0, Lunitek SrL, Sarzana, Italy, with a frequency range of 15–625 kHz) positioned at the exact center of the sample, along with a data acquisition system using a sampling frequency of 5 MHz and storing the data in a parametric format, for damage detection; and digital image correlation (DIC) to monitor strain distribution in the samples, utilizing two monochrome cameras (VIC-EDU System) set to capture images every 2 seconds under optimal lighting and focus, with data analysis conducted using VIC-3D software (both from Correlated Solutions®).

In a parallel procedure, a fragment consisting of a single layer of the repaired sample and subsequently brought to break was also tested by THz time-domain spectroscopy (THz-TDS) with TeraSmart® system by MenloSystems.

2.3 Testing procedure

Following the application of the acoustic emission sensor with a two-component resin, the DIC pattern was set up with a thermal painting and a toothbrush. Subsequently, the sample was positioned on the testing apparatus for the tensile test, and the appropriate brightness and focus of the DIC were adjusted. Upon completion of preparations, the tensile test started alongside the simultaneous acquisition of acoustic emission and digital image correlation data.

The tensile test was conducted in displacement control mode, setting the velocity of the hydraulic jack to 0.05 mm/sec. The sample was subsequently subjected to a force increment from zero up to 25 kN and then decreased to zero, with two repetitions. It is worth noting that during the repetitions/loading steps, the sample was not removed from the tensile machine (Figure 2). Upon completion of the test on the now-damaged virgin sample, after detaching the AE sensor, the sample underwent a repairing process in oven at the temperature of 135°C for 5 minutes. The AE sensor was re-attached at the same location on the repaired sample using two-component resin, and the prior procedure was subsequently reiterated.

3 RESULTS

Below are shown the main test results broken down by the analysis technique used.

3.1 Tensile test

Figure 3 shows the load - unload sequence for the virgin and repaired versions of the sample (Load 1 and Load 2 indicate the two consecutive loading steps).

Figures 4a and 4b show the load vs displacement curves for the virgin and repaired versions of the sample, respectively

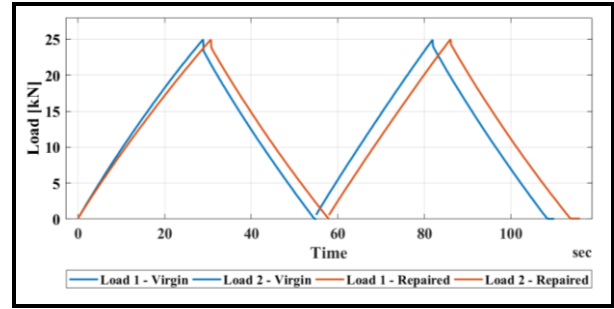


Figure 3: Load - time of the tensile test.

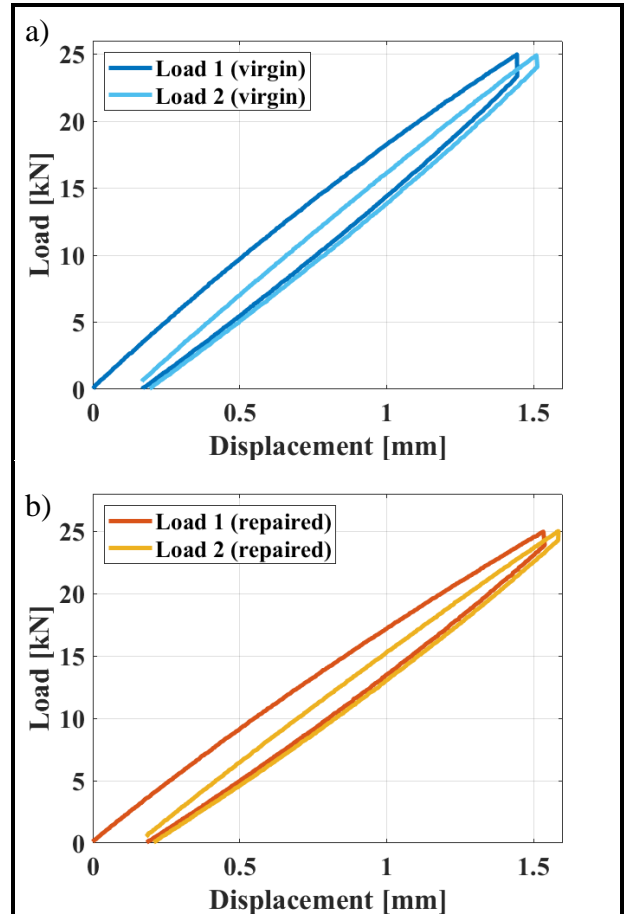


Figure 4: Load-displacement response from the tensile test for the virgin (a) and repaired (b) versions.

The responses of the virgin and repaired versions are compared in Figure 5, where the curves are grouped by load steps. In the same figure, the areas enclosed in the load - displacement curves are highlighted with indication of their measures. We can observe that: (i) for each load step, the areas of the virgin and repaired versions are similar; and (ii) the area enclosed in Load 2 step is smaller than that of Load 1 step.

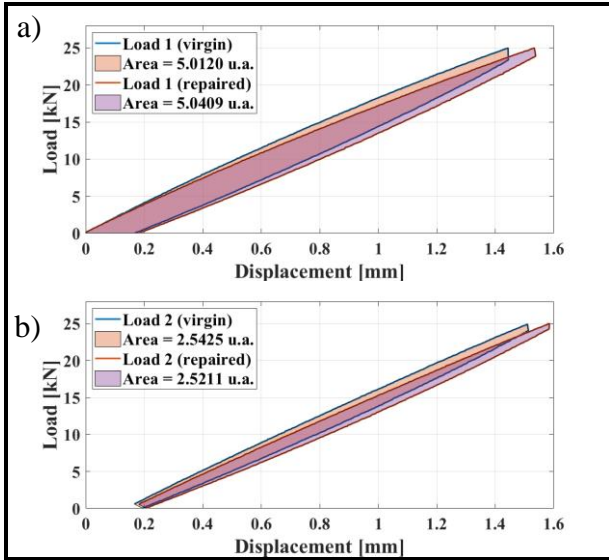


Figure 5: Load-displacement response and area for the Load 1 (a) and Load 2 (b) steps. (u.a. = unity of area).

The results from tensile test also show that the sample holds a residual deformation after each unload. This holds both for the virgin and repaired versions. Moreover, it can be noted that the repaired sample shows a lower stiffness compared to its virgin version (Figure 5).

3.2 Acoustic emission (AE)

To analyze the evolution of the AE signal during the tensile test, a threshold amplitude of 6.7 mV was established. Figures 6 and 7 show the load and the accumulated AE signals plotted vs time for the virgin and repaired versions, respectively.

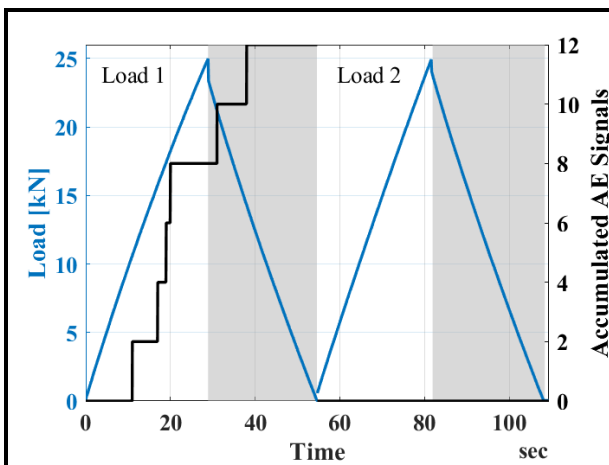


Figure 6: Accumulated AE Signals for the virgin sample.

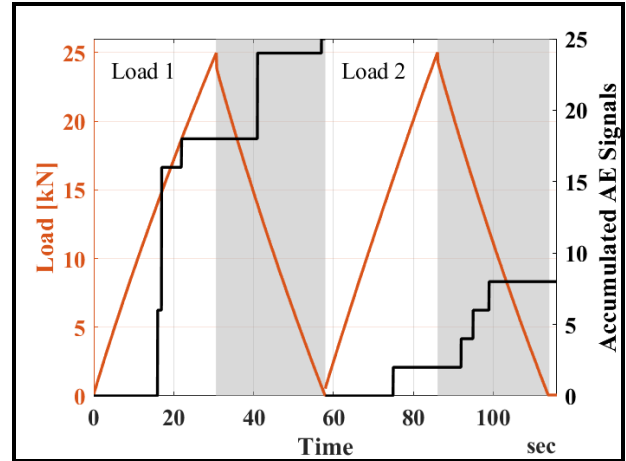


Figure 7: Accumulated AE signals for the repaired sample.

For each version of the sample, Load 1 step exhibits more AE activity than Load 2 step, highlighting the absence of AE signals in the Load 2 step for the virgin sample (Figure 6). Furthermore, when considering the AE activity for both the virgin and repaired versions, it is evident that the repaired version displays a greater number of AE signals compared to the virgin case. Specifically, the repaired version presents a total of 33 (25 + 8) cumulative AE signals, while the virgin version shows only 12 (12 + 0) cumulative AE signals.

3.3 Digital image correlation (DIC)

For the post-processing in VIC-3D, for each specimen the area of interest (green area in Figure 8) was defined, then within it three other sub-areas (top, center, down) were identified and two virtual strain gauges added: one longitudinal of length 80 mm and one transversal of length 10 mm. The region designated for strain calculation was effectively divided into subsets of sufficient size to encompass enough distinctive pattern information, differentiating it from adjacent areas. Given the small dimension of the speckle, the subset size was determined to be 29. The step size, which dictates the pixel distance between each data point, was established at 1 (the minimum) to increase the number of data points, even though this resulted in a longer analysis duration. The final operation involved establishing the initial point for the analysis, ensuring that correlation

could be effectively applied, which was situated in an area of minimal movement, near the top grip. Strains were calculated using the Lagrange tensor.

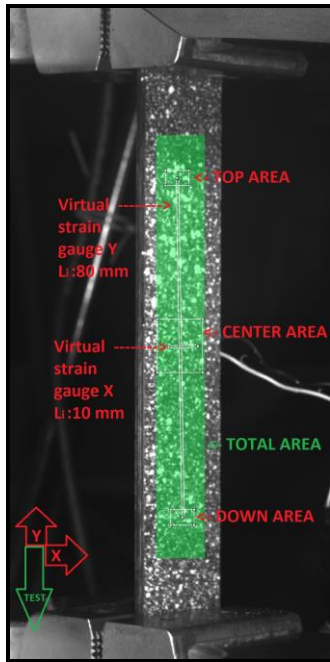


Figure 8: Detail of test setup and apparatus.

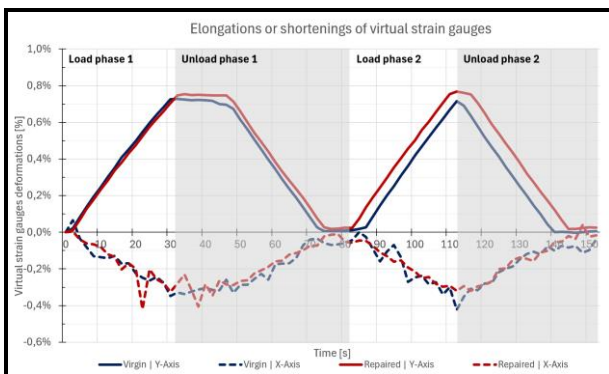


Figure 9: Elongations or shortenings of virtual strain gauges over time.

Figure 9 shows the percentage elongations and contractions of the virtual strain gauge during the test. Figure 10 displays the longitudinal strains for the entire area, along with the upper, central, and lower sections. In both figures, the values for the unaltered (virgin) specimen are in blue, while the repaired specimen values are in red. The average values are represented by a solid line, while the maximum values recorded in the analysis area at that specific moment are

indicated by a dotted line. The four phases of the test have been delineated into white and grey areas, specifically: loading at 25 kN, unloading, reloading at 25 kN, and finalizing the unloading process.

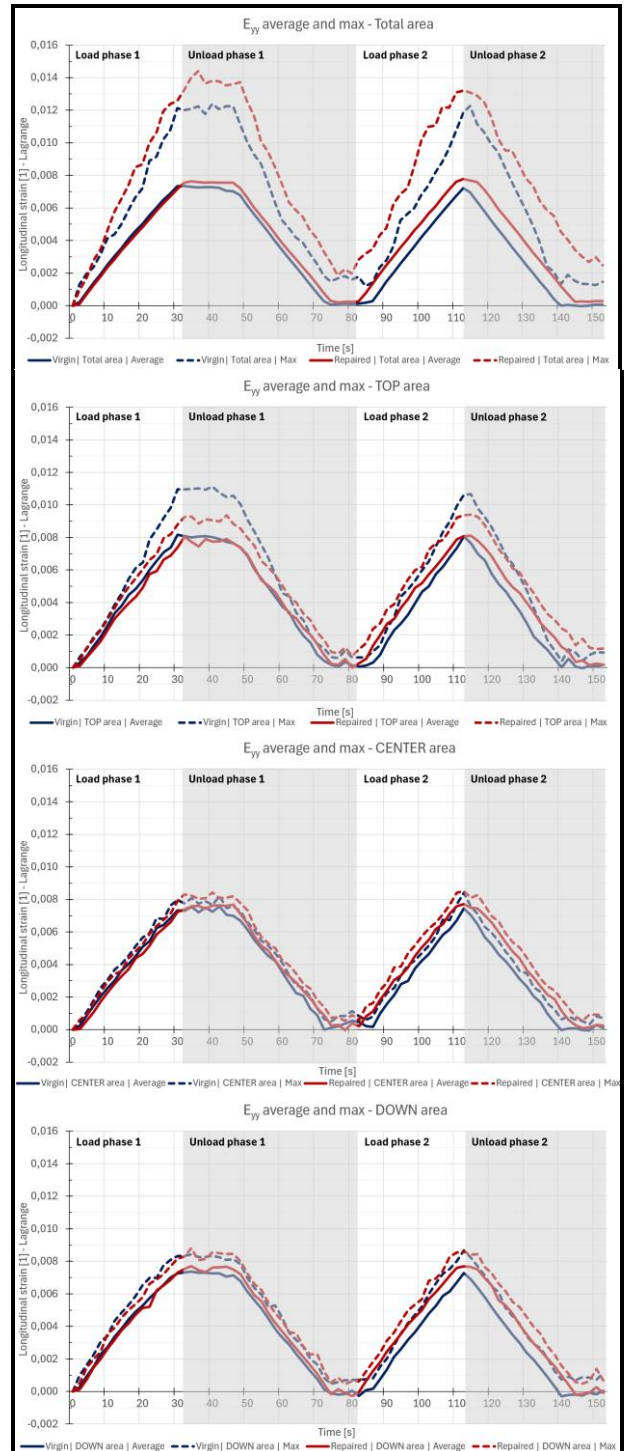


Figure 10: Longitudinal strain (E_{yy}) value over time, from top to bottom respectively total area of interest, top area, center area, down area.

4 DISCUSSIONS

As previously shown in Figure 3, the force was applied and removed twice in the tensile test. From the Figures 4 and 5 it is possible to verify that the sample holds a residual deformation after each stage of applied force, both before and after the repair process. Moreover, the stiffness of the repaired version is lower than that of the virgin version.

Concerning the analysis of AE signals, it can be noted that a bigger AE activity was recorded for the repaired version. The reason of this behavior is not clear yet, and further investigations are needed.

Concerning the elongations along the Y-axis, it was evident that during load phase 1, the trend of the repaired sample aligns with that of the virgin sample. The repaired sample exhibits a marginally elevated percentage of deformation, indicating residual deformation consistent with the tensile test results. The elongation along the Y-axis in load phase 2, in terms of percentage and behavior, aligns with phase 1. Upon completion of the tests on the repaired samples, a residual deformation of approximately 0.03% is observed. The recorded shortenings along the X-axis of the virtual extensometer are less linear than those along the Y-axis; this can be ascribed to both the small size of the cross-section and the fact that the transverse virtual extensometer pertains to a specific section of the sample.

A detailed analysis of the longitudinal deformations reveals that the average deformations align with the elongations observed in the virtual extensometer depicted in Figure 8. Moreover, throughout the entire region, the repaired sample exhibited higher deformation peaks than the virgin sample, attaining deformations of 0.014 (1.4%). The sample repaired in load phase 2 exhibited a maximum deformation of 1.3%, which is marginally larger than that of the virgin sample (1.2%). Upon analyzing the center and down sub-areas, it is evident, particularly in load phase 1, that the repaired sample exhibits a deformation consistent with that of the virgin sample, thereby underscoring the repair that has occurred. A comparable phenomenon

transpired in the top sub-area, where there was a decrease in the maximum deformations of the repaired sample, diminishing from a peak of 1.1% to approximately 0.9%, thereby indicating an enhancement (recover) in local performance attributable to the repair (note that maximum strains do not necessarily occur at the same point).

In anticipation of future investigations, Figure 11 shows the THz power spectrum (in transmission setup) of the center point of the fragment, showing the highest peak at 0.29 THz; on the right, a 2D image of the whole fragment at that specific frequency is shown.

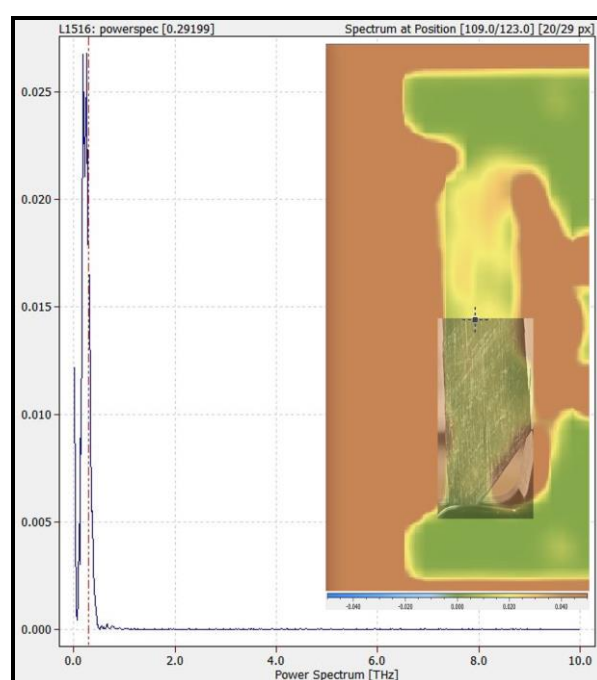


Figure 11: THz fragment power spectrum and 2D image at 0.29 THz.

5 CONCLUSIONS

According to the findings, local repair of the healable composite material under investigation, made of a polymer matrix and carbon fibers, was detected when it has been firstly damaged and then subjected to heat treatment. This accurate assessment was possible because we have incorporated different investigative methods able to catch information at the meso- and micro-level, such as AE and DIC. Conversely, the sole global observation of the results of tensile tests does not appear to indicate that this behavior is

occurring. The subsequent stages of the investigation will involve the testing of additional sample geometries and the incorporation of other investigative methods, such as THz spectroscopy, both in transmission and reflection setup, which is currently being carried out for the purpose of better interpretation of the repairing mechanism.

REFERENCES

- [1] Jee Kanu, N., Gupta, E., Kumar Vates, U., Kumar Singh, G., 2019. Self-healing composites: A state-of-the-art review. *Composites Part A: Applied Science and Manufacturing*. **121**: 474-486.
- [2] Beiermann, B. A., Keller, M. W., Sottos, N. R., 2019. Self-healing flexible laminates for resealing of puncture damage. *Smart Mater. Struct.* **18**:085001.
- [3] Shiotani, T., Ogura, N., Okude, N., Watabe, K., Van Steen, C., Tsangouri, E., Lacidogna, G., Czarnecki, S., Chai, H.K., Yang, Y., Verstryngge, E., Aggelis, D.G., 2024. Non-destructive inspection technologies for repair assessment in materials and structures. *Developments in the Build Environment*. **18**:100443.
- [4] Brown, E. N., Sottos, N. R., White, S. R., 2002. Fracture Testing of Self-Healing Polymer Composite. *Experimental Mechanics*. **42**:372-379.
- [5] Al-Nadhari, A., Yildirim, C., Topal, S., Tabrizi, I. E., 2025. In-situ acoustic emission based technique for damage detection and identification and failure mode prediction in scarf repaired composite structures. *Measurement*. **242**:116068.
- [6] Saeedifar, M., Najafabadi, M. A., Yousefi, J., Mohammadi, R., Toudeshky, H. H., Minak, G., 2017. Delamination analysis in composite laminates by means of Acoustic Emission and bi-linear/tri-linear Cohesive Zone Modeling. *Composite Structures*. **161**:505-512.
- [7] Ruiz, O. G., Reinoso, M. R., Ingrassia, E., Vecchio, F., Maniero, F., Burgio, V., Civera, M., Bitan, I., Lacidogna, G., 2022. Design and Mechanical Characterization Using Digital Image Correlation of Soft Tissue-Mimicking Polymers. *Polymers*. **14**:2639.